Supporting Information for

Unexpectedly resisting protein adsorption on self-assembled monolayers terminated with two hydrophilic hydroxyl groups

Dangxin Mao, Yuan-Yan Wu[*], and Yusong Tu[*]

College of Physics Science and Technology, Yangzhou University, Jiangsu 225009, China
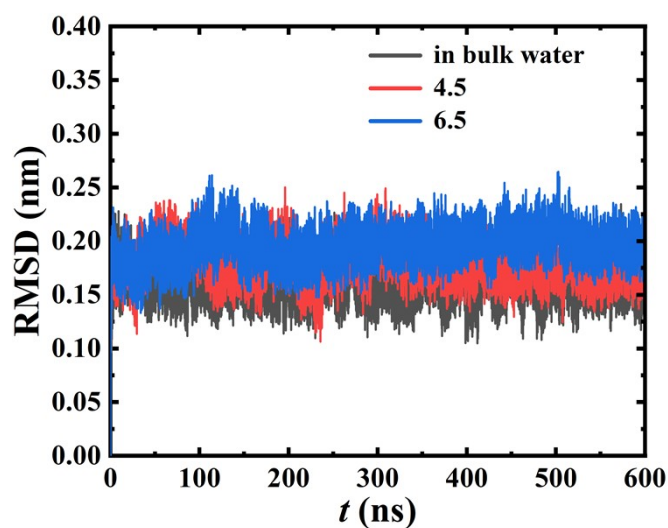
[*]Corresponding author: yywu@yzu.edu.cn; ystu@yzu.edu.cn

Fig. S1 The protein backbone RMSD at Σ = 4.5 nm^{-2} (red line), 6.5 nm^{-2} (blue line), and in bulk water (black line), respectively.
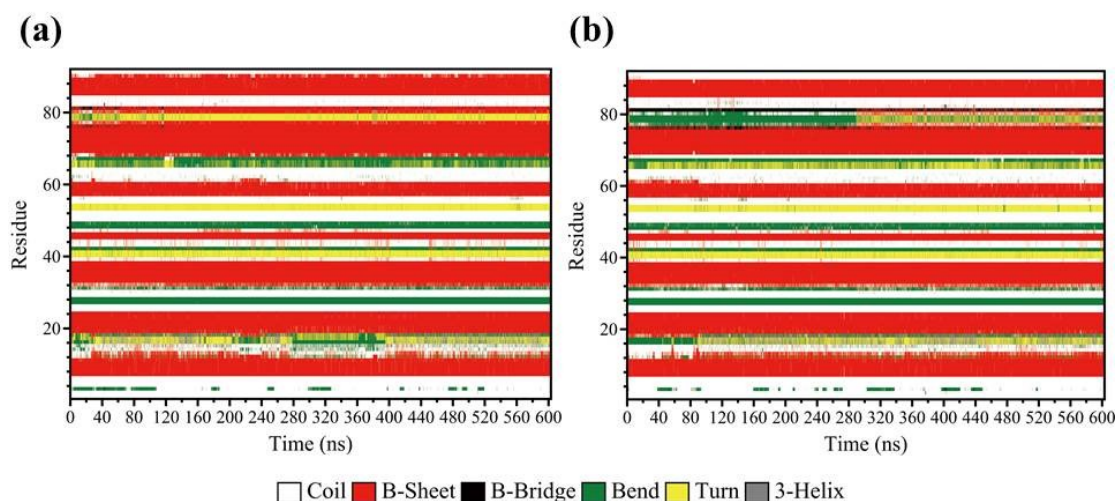
Fig. S2 The secondary structure evolution of protein at $\Sigma = 4.5$ nm^{-2} (a), 6.5 nm^{-2} (b). The β-sheets are shown in red.
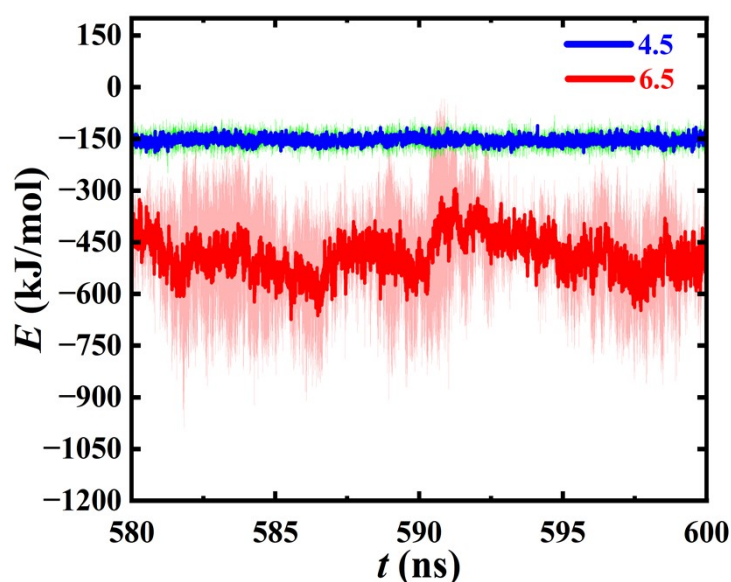

Fig. S3 The electrostatic interactions between protein and the (OH)$_2$-SAM at $\Sigma = 4.5$ nm^{-2} (blue line) and 6.5 nm^{-2} (red line) for the last 20ns, respectively. The error bars are indicated by green areas ($\Sigma = 4.5$ nm^{-2}) and light red areas ($\Sigma = 6.5$ nm^{-2}), respectively.

The electrostatic interactions between protein and the (OH)$_2$-SAM were calculated to characterize the binding strength of protein adsorption on the (OH)$_2$-SAM. As shown in Fig. S3, the average interaction energies at $\Sigma = 4.5$ nm^{-2} are stable around -150 kJ/mol, which is much weaker than those at $\Sigma = 6.5$ nm^{-2}, further indicating that the stable and strong resistance to protein adsorption exhibited by the structure of (OH)$_2$-SAM itself.
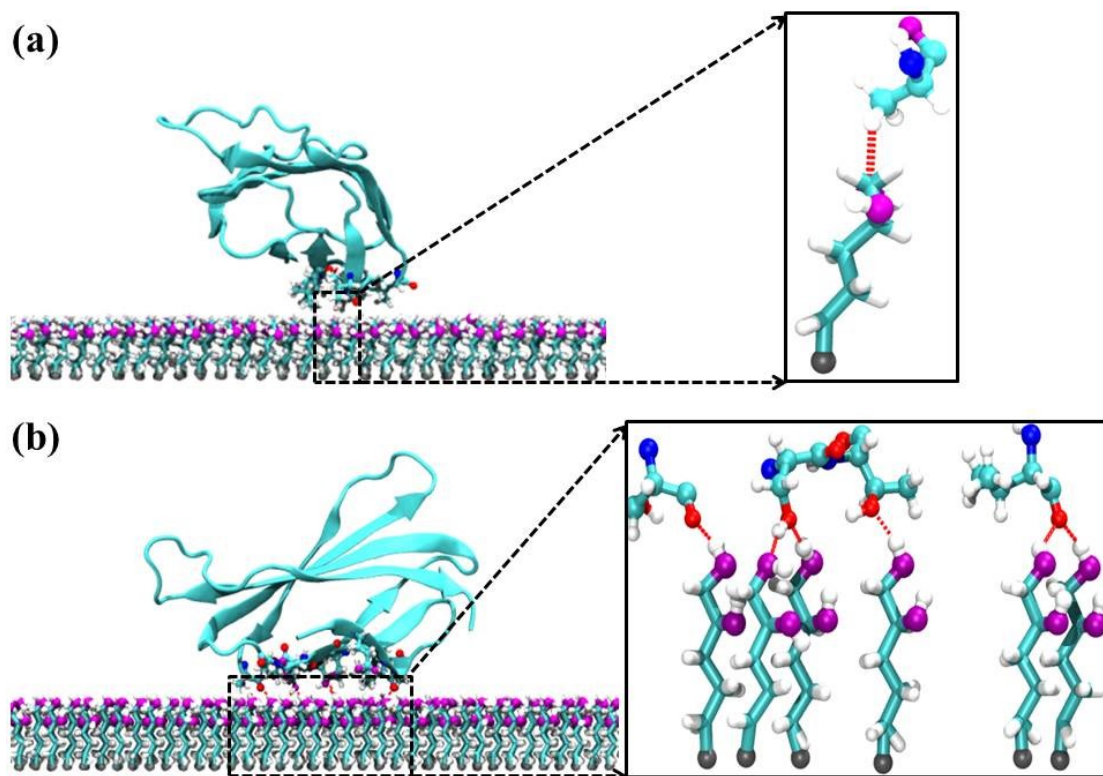
Fig. S4 The representative snapshots of the side view of protein adsorption on the (OH)$_2$-SAM at Σ = 4.5 nm^{-2} (a), 6.5 nm^{-2} (b). The H-bonds formed between the protein residues (ball and stick mode) and the alkyl chains are indicated by red dashed lines in the insets. The atom representations and color settings are as in Fig. 1.
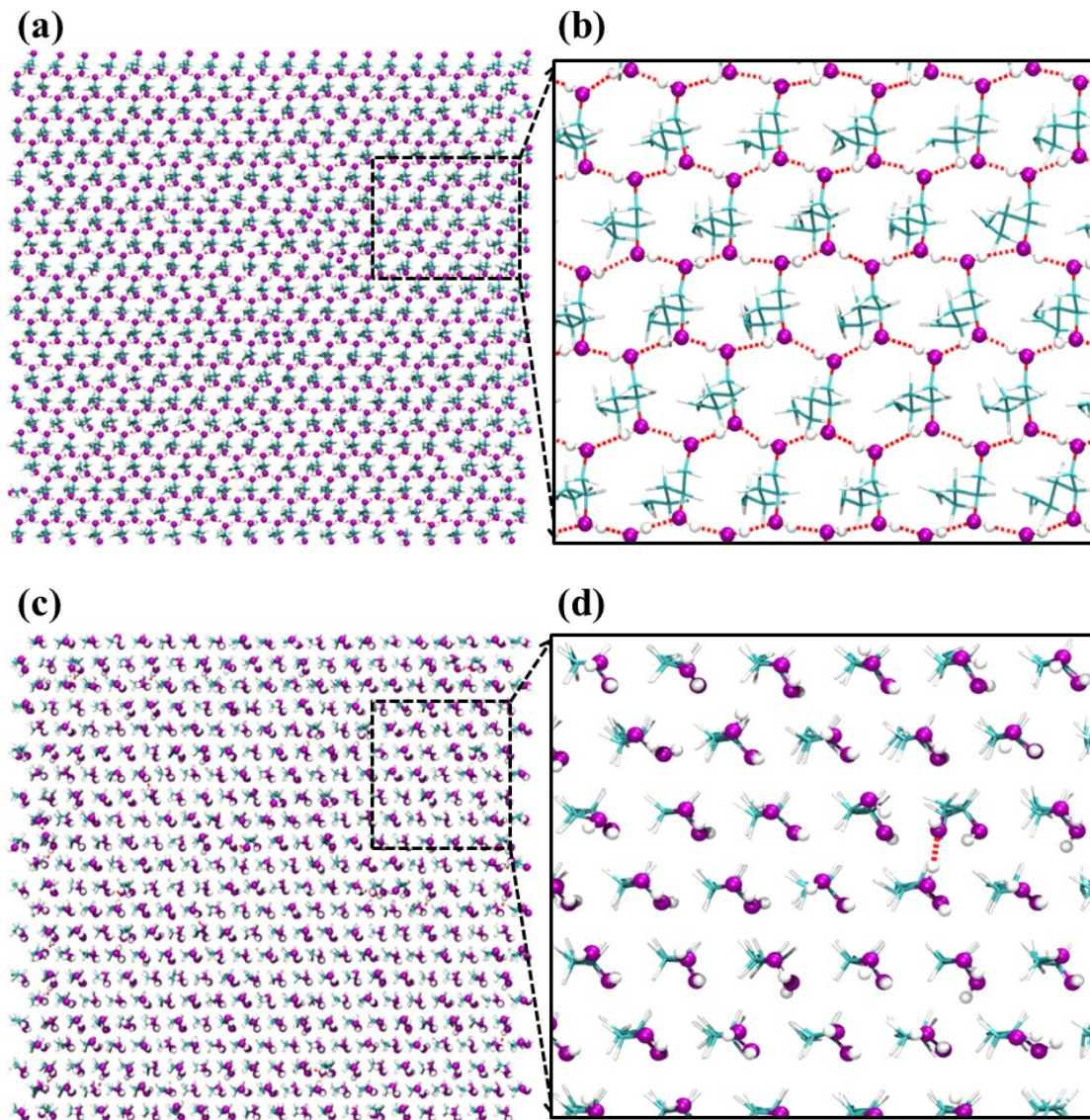
Fig. S5 (a) The simulation snapshot of the top view of the $(OH)_2$-SAM at $\Sigma = 4.5$ nm^{-2}, (b) and the subfigure with the hexagonal-ice-like H-bond structure in the OH matrix of the $(OH)_2$-SAM. (c) The simulation snapshot of the top view of the $(OH)_2$-SAM at $\Sigma = 6.5$ nm^{-2}, (d) and the subfigure with the state of H-bond formation in the OH matrix of the $(OH)_2$-SAM. The atom representations and color settings are the same as the previous.

Table S1 H-bond number analysis for protein (1FNA) at $\Sigma = 4.5$ nm^{-2} and 6.5 nm^{-2}

Σ (nm^{-2})	SAM-SAM	SAM-water	SAM-protein
4.5	8.0 ± 0.01	2.8 ± 0.02	0.2 ± 0.11
6.5	2.1 ± 0.02	7.0 ± 0.02	4.4 ± 0.77

The protein exhibits a net charge of +6 e in our simulation, and we also select another fibronectin (PDB code: 1FNA[1]) with a net charge of 0 to increase the representativeness of the protein. We analyze the average number of H-bonds in the

OH groups of the $(OH)_2$-SAM (SAM-SAM, Table S1), between the $(OH)_2$-SAM and water (SAM-water, Table S1), and between the $(OH)_2$-SAM and protein (SAM-protein, Table S1) to confirm the validity of the key conclusions in our study. As shown in Table S1, the results are highly consistent with those in our main text. It can be seen from Table S1 that the number of H-bonds between the $(OH)_2$-SAM and protein at $\Sigma = 6.5$ nm^{-2} is still ~8 times higher than that at $\Sigma = 4.5$ nm^{-2}, indicating the robustness of strong resistance to protein adsorption exhibited by the structure of the $(OH)_2$-SAM itself at $\Sigma = 4.5$ nm^{-2} compared to that exhibited by traditionally physical barrier effect formed by a large number of H-bonds between the $(OH)_2$-SAM and water at $\Sigma = 6.5$ nm^{-2}. Fig. S4 also shows the difference in protein adsorption on the $(OH)_2$-SAM at the two pcaking densities. The excellent resistance to protein adsorption is exhibited by the structure of $(OH)_2$-SAM itself, i.e., the stable hexagonal-ice-like H-bond structure (Fig. S5b) with 8.0 ± 0.01 nm^{-2} H-bond numbers at $\Sigma = 4.5$ nm^{-2} while few H-bonds are formed in the OH groups at $\Sigma = 6.5$ nm^{-2} (Fig. S5d), indicating that the structure of $(OH)_2$-SAM itself plays a key role in resisting protein adsorption. These analyzes show that our conclusions remain unchange regardless of changes in protein charge, indicating the validity and robustness of our conclusions.

Table S2 The force field parameters for $(OH)_2$-SAM

| atom name	charge (e)	sigma (Å)	epsilon (kcal/mol)
OH	-0.683	0.312000	0.711280
HO	0.418	0.000000	0.000000
CT1	-0.18	0.350000	0.276144
HC1	0.06	0.250000	0.125520
HC2	0.06	0.250000	0.125520
CT2	-0.12	0.350000	0.276144
HC3	0.06	0.250000	0.125520
CT3	-0.12	0.350000	0.276144
HC4	0.06	0.250000	0.125520
HC5	0.06	0.250000	0.125520
CT4	0.205	0.350000	0.276144
HC6	0.06	0.250000	0.125520
HC7	0.06	0.250000	0.125520
CT5	0.145	0.350000	0.276144
HC8	0.06	0.250000	0.125520
HC9	0.06	0.250000	0.125520
OH2	-0.70	0.307000	0.711280
HO2	0.435	0.000000	0.000000
CA	0.06	0.355000	0.292880
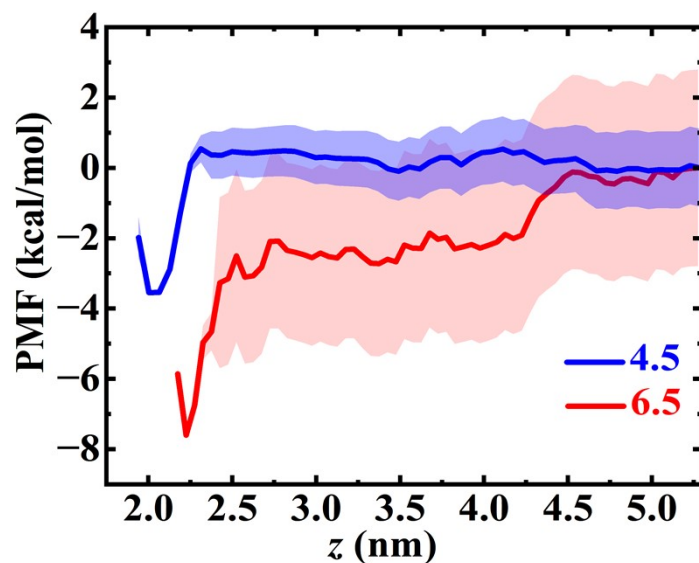
Fig. S6 The PMF profiles for protein along the reaction coordinate (z-axis) using the MBAR method at $\Sigma = 4.5$ nm^{-2} (blue line) and 6.5 nm^{-2} (red line), respectively. The error bars are indicated by light blue areas ($\Sigma = 4.5$ nm^{-2}) and light red areas ($\Sigma = 6.5$ nm^{-2}), respectively.

As shown in Fig. S6, the average PMF values are highly consistent with those calculated by the WHAM method. Also, the average PMF values at $\Sigma = 6.5$ nm^{-2} were more negative, and the difference between the well depth of the average PMFs is still nearly ~4 kcal/mol, indicating the robustness of our conclusions.

References

1 C. D. Dickinson, B. Veerapandian, X. P. Dai, R. C. Hamlin, N. H. Xuong, E. Ruoslahti and K. R. Ely, *J. Mol. Biol.*, 1994, **236**, 1079-1092.